

Valence excitation of NO_2 by impulsive stimulated x-ray Raman scattering

Daniel J. Haxton¹

¹Department of Physics, University of California, Berkeley CA 94720

Impulsive x-ray Raman excitations are the components of multidimensional x-ray spectroscopies that have been proposed. However the question of the optimum laser parameters to use for these impulsive excitations is still open. Impulsive x-ray Raman valence excitations of the NO_2 molecule driven by 1fs pulses tuned below the Oxygen K-edge were calculated in the fixed-nuclei approximation using the multiconfiguration time-dependent Hartree-Fock (MCTDHF) method. Fixing the duration but varying the central frequency and intensity of the pulse, not considering chirp, maximum population transfer is obtained at an intensity of approximately $3 \times 10^{17} \text{ W cm}^{-2}$, with the central frequency substantially 8eV red-detuned from the 2nd order optimum, and most likely driven by nonresonant Raman with the Oxygen K-edge continuum. Strong nonlinear effects are present at $10^{16} \text{ W cm}^{-2}$. The results will hopefully help guide the selection of experimental conditions under which multidimensional X-ray spectroscopies are most viable.

PACS numbers: 33.20.Fb 33.20.Rm 42.65.Re 42.65.Dr

I. INTRODUCTION

Recent proposals for using ultrafast x-ray pulses to study valence electron and hole motion in molecules [1, 2] rely on the creation of a coherent valence electronic wavepacket using two-photon, Raman transitions. Ultrafast, even attosecond broadband x-ray pulses drive the impulsive stimulated Raman process, the excitation via the pump frequencies and the stimulated emission of Stokes frequencies, leading to a coherent valence excitation. The 1D- and 2D-SXRS multidimensional spectroscopies [1, 2] employ multiple impulsive Raman excitations in order to obtain information about electronic structure and couplings and the internuclear geometry. There have been several sophisticated theoretical and computational studies of multidimensional X-ray spectroscopic and related methods including Refs. [3–5].

However, these studies have often concentrated on electronic excitations to metastable core-excited states and neglected the continuum above the edge [6], and often they have explicitly computed the nth-order signal without considering large-magnitude higher-order behavior that might overwhelm lower orders even at low intensity. It is desirable to test the efficiency of the atomic impulsive stimulated x-ray Raman transitions in polyatomic molecules, in a fully nonperturbative, first-principles calculation that accounts for all the fundamental effects including multiple ionization, stark shifts, and highly correlated electronic dynamics. The Multiconfiguration time-dependent Hartree-Fock (MCTDHF) method is capable of calculating arbitrary nonperturbative quantum dynamics of electrons in medium-sized molecules. We have applied our implementation of it [7–10] to predict valence population transfer due to stimulated X-ray transitions in the NO_2 molecule, in the fixed-nuclei approximation.

We show that in the NO_2 molecule, for impulsive stimulated x-ray Raman scattering using 1fs pulses, transitions to the $^2\text{B}_1$ valence electronic state dominate. Population transfer of about 10^{-3} (a 3% coherence) may

be driven at 2nd order by tuning below the near-edge fine structure, as in Ref. [6]. However, nonlinear effects quickly set in above $10^{16} \text{ W cm}^{-2}$, and a global optimization of population transfer as a function of intensity and central frequencies occurs with significant red detuning and appears to be driven by nonresonant Raman transitions through the continuum above-edge.

II. MCTDHF CALCULATION OF NO_2

Our implementation of MCTDHF [10] for electrons in molecules has already been described [7–9]. Briefly, the MCTDHF method [11–25] solves the time-dependent Schrodinger equation using a time-dependent linear combination of Slater determinants, with time-dependent orbitals in the Slater determinants. The nonlinear working equations are obtained through application of the Lagrangian variational principle [26, 27] to this wave function ansatz.

The representation of orbitals using sinc basis functions is described in Ref. [9]. For NO_2 , we use a grid of $55 \times 55 \times 55$ ($= 166375$) product sinc basis functions for the orbitals. The spacing between the functions is 0.2975614 bohr (about 0.56 Angstrom). The calculations are performed with full configuration interaction, 23 electrons in 15 orbitals, giving 621075 Slater determinants which are contracted to 305760 spin-adapted linear combinations and distributed among processors. The mean field time step was 0.02 atomic time units (approximately one half attosecond).

Complex coordinate scaling and stretching [28] is applied starting at ± 4 bohr in the x , y , and z directions. We perform the smooth complex scaling transformation upon the kinetic energy and derivative operators only. Lacking a viable method for defining the transformed two-electron operator, we do not transform the Coulomb operators. (We have found that this approximation, neglecting to transform the Coulomb operators, gives sharp ionization edges with truncated Rydberg series.) The complex ray

is defined as

$$\begin{aligned}
X(x) &= x + a(x - x_0) + b \sin\left(\pi \frac{x - x_0}{x_1 - x_0}\right) \\
&\quad + c \sin^3\left(\pi \frac{x - x_0}{x_1 - x_0}\right) \quad (x_0 \leq x \leq x_1) \\
&= x + a(x + x_0) + b \sin\left(\pi \frac{x + x_0}{x_1 - x_0}\right) \\
&\quad + c \sin^3\left(\pi \frac{x + x_0}{x_1 - x_0}\right) \quad (-x_1 \leq x \leq -x_0) \\
&= x \quad (-x_0 \leq x \leq x_0)
\end{aligned} \tag{1}$$

in which $X(x)$ defines the complex coordinate ray X along which the wave function is defined as a function of the real-valued parameter x in which the operators are represented. Smooth scaling occurs between the scaling boundary $x_0 = 4a_0$ and the end of the grid $x_1 \approx 8.78a_0$. The parameters a , b , and c are determined by the scaling angle and stretching factor (half a radian and three, respectively, such that $X'(x) = 4e^{0.5i}$ at $\pm x_1$) and by making the fourth derivative $X'''(x)$ continuous. This transformation defines the new length-gauge dipole operators X , Y , and Z , and the dvr weights in each Cartesian direction (originally uniformly $w_i = \frac{1}{\Delta}$ with Δ the sinc DVR spacing) are modified according to $w_i \rightarrow X'(x_i)w_i$. The first derivative operator matrix elements are transformed as e.g. $(d/dX)_{ij} = (d/dx)_{ij}(X'(x_i)X'(x_j))^{-1/2}$, and the kinetic energy matrix elements are defined in the DVR approximation as

$$\begin{aligned}
\left(\frac{\partial^2}{\partial X^2}\right)_{ij} &= \frac{1}{X'(x_i)X'(x_j)} \left(\frac{\partial^2}{\partial x^2}\right)_{ij} \\
&\quad - \delta_{ij} \frac{3X''(x_i)^2 - 2X'''(x)X'(x_i)}{4X'(x_i)^4}
\end{aligned} \tag{2}$$

We calculate population transfer for the valence B_1 , B_2 , and A_2 states. We integrate the result over orientations using Lebedev quadrature. Comparing 38- and 50-point quadrature, we find that most of the results are converged with 38-point quadrature. We have not attempted to demonstrate the convergence of these results beyond 50-point quadrature due to computer resources. In Figure 1 we show the convergence of the B_1 population at $10^{17} \text{ W cm}^{-2}$, with respect to the order of the Lebedev quadrature.

Due to symmetry, and within the rotating wave approximation, only seven of the 50 points need to be calculated. Each central frequency and intensity required approximately 10,000 cpu-hours to calculate: seven calculations, 121 processors each, and about twelve hours per calculation.

The energies of the valence states are shown in Table I. We provide vertical transition energies from the literature, and also report our transition energies. These are the transition energies of the states used for projection, relative to the initial state used in the MCTDHF propagation. The states are not used in the MCTDHF calculation, and we have demonstrated [29] that these transition energies do not correspond with transition energies apparent from MCTDHF calculations. They are nevertheless included here for the sake of completeness.

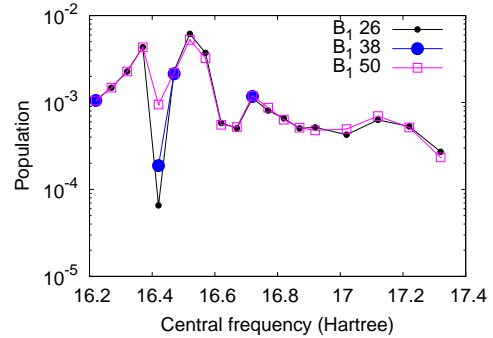


FIG. 1. (Color online) Convergence of the B_1 population at $10^{17} \text{ W cm}^{-2}$, with respect to the order of the Lebedev quadrature used for the orientation average of fixed-nuclei calculations.

	Ref. [30]	Present
B_1	2.827 eV	4.294 eV
B_2	3.239 eV	3.850 eV
A_2	3.977 eV	4.009 eV

TABLE I. Transition energies for valence states: vertical transition energies previously calculated from Ref. [30], and transition energies for states used to define populations from the MCTDHF calculation.

Due to the spacing of sinc functions – again, 0.2975614 bohr – and the fact that we have not elaborated our method with any pseudopotential or effective theory to account for the truncation in momentum space, the core transitions that drive the X-ray Raman process are shifted substantially downward in energy. As can be seen in Fig. 2, the Oxygen K-edge appears at approximately 470eV in these calculations, not the actual 540eV.

Fig. 2 shows the photoionization cross section calculated in the neighborhood of the Oxygen K-edge. The magnitude of the cross section above and below the edge (about 0.5 and a bit more than 1.0 respectively) agree

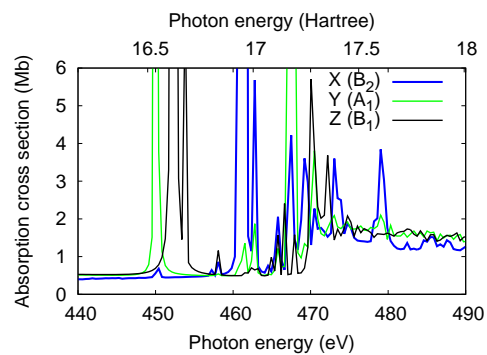


FIG. 2. (Color online) NO_2 photoionization cross section calculated in the vicinity of the Oxygen K-edge using a 10fs MCTDHF calculation with a weak pulse. The K-edge is artificially low in these calculations.

well with figure 5.10 in Berkowitz's compilation [31]. The three peaks at about 450 (A_1), and 452 & 453 (B_1) correspond to excitations to $6a_1$ and $2b_1$ from the Oxygen 1s σ_g orbital, and correspond with the peaks observed at approximately 530, 532, and 533 in experiment [32–34]. Relative to these peaks, there is also a pair of B_2 states, at about 462eV, both spin couplings for excitation to $5b_2$, and the K-edge lies at about 468eV. It is clear that the K-edge is too high in energy, and the B_2 states are too low, because the B_2 states are observed as a broad core-excited shape resonance in experiment. Experiment [32–34] gives a A_1 to B_2 excitation energy of 15eV, and a K-edge about 12eV above A_1 ; here they are found at about 12 and 18eV, respectively.

III. RESULTS FOR IMPULSIVE X-RAY RAMAN EXCITATION OF NO₂

The results for population transfer using 1fs linearly polarized pulses are shown in Figure 3.

The best population transfer is obtained for the B_1 state, at approximately 3×10^{17} W cm⁻², substantially red-detuned from the second-order optimum. However the optimum population transfer is only 1% with these one-femtosecond, linearly polarized pulses. We will vary chirp and duration in future work.

The second-order behavior is visible in Fig. 3 in the bold black line with open squares, corresponding to intensity 1×10^{15} W cm⁻². This result has been multiplied by 100 in the figure, and lies on top of the orange (grey) line with solid squares in the figure, the line corresponding to intensity 1×10^{16} W cm⁻², on the left-hand side of the figure at lower central frequency. Thus, one can see that even at 1×10^{16} W cm⁻², when the central frequency is low such that the pulse is not resonant with any of the near-edge fine structure nor the continuum above the edge, the behavior is still second-order.

However, as the intensity is increased, strong nonlinear effects arise that are contrary to the conventional wisdom. We see here that the optimum population transfer is obtained with central frequency much different from the the second-order optimum. In Fig. 3, we see that as the intensity is increased, a strong minimum in the population transfer for the B_1 and A_2 states develops around 447eV in these calculations. This minimum persists for a range of intensities. Among the calculations we have performed, the overall optimum population transfer is seen to occur to the B_1 state, below this robust minimum, at 3.16×10^{17} W cm⁻², and a central frequency of 444eV in these calculations. 444eV is approximately 6eV below the lowest state responsible for the near-edge fine structure, the A_1 excitation $1s \rightarrow 6a_1$, and 8eV below the 2nd order optimum.

We plan further calculations and modeling to interrogate the nature of this excitation. However, it seems clear from the results that this excitation is driven by nonresonant Raman via the $1s^{-1}$ continuum. For each of the

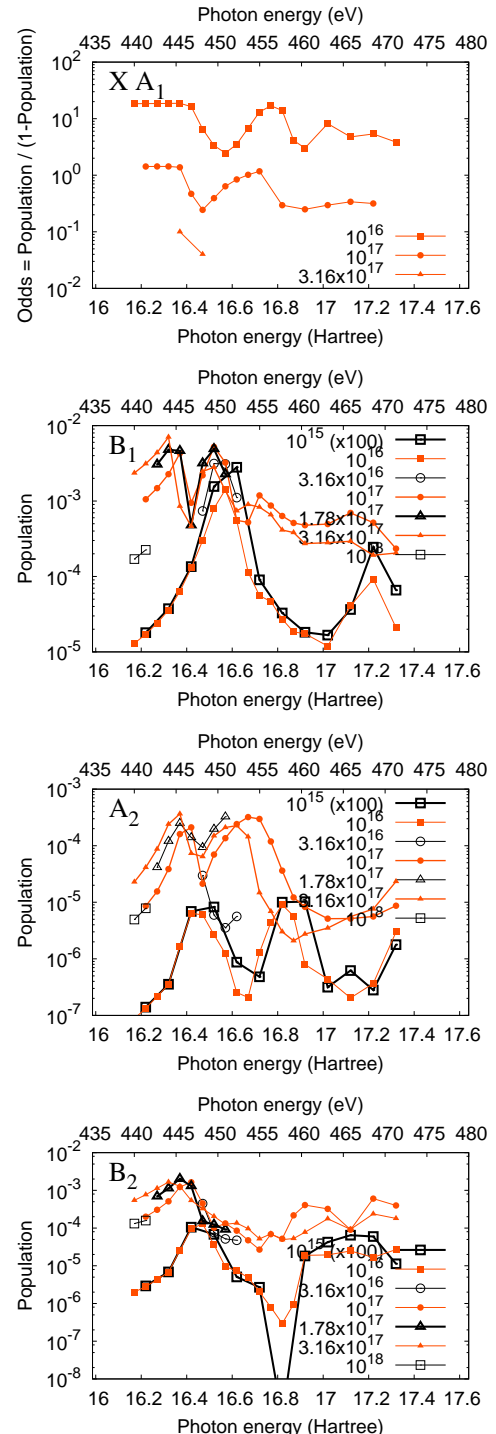


FIG. 3. (Color online) Results for population transfer to the B_1 , A_2 , and B_2 valence excited states of NO₂, and odds for remaining in the ground state, averaged over orientation, for 1fs pulses, as labeled. Different intensities are plotted with different lines and labeled in Watts per square centimeter.

three states, the excitation probability drops steeply as the central frequency is decreased on the left side of the figures. This behavior is what we would expect from nonresonant Raman via the Oxygen $1s^{-1}$ continuum at higher energy. In contrast, if population transfer were occurring via direct, one-electron Raman, or via the continuum excitations of the $2s$ or $2p$ electron(s) or the $1s$ electrons of Nitrogen, we would expect relatively constant behavior on the left side of the figure.

IV. CONCLUSION

Using an implementation of the MCTDHF method which is in principle of calculating an accurate solution to the Schrodinger equation including nonrelativistic electronic effects for polyatomic molecules, we have provided a survey of population transfer to valence electronic states in NO_2 by linearly polarized 1fs pulses tuned near the Oxygen K-edge. Such impulsive x-ray Raman transitions underly proposed methods of multidimensional x-ray Raman spectroscopies [1, 2], and x-ray pulses of the required coherence, synchronization, and intensity will soon be available with developments in next-generation light sources or high harmonic generation.

Most theoretical and computational treatments so far have not considered continuum oscillator strength that may drive the process, and many have been perturbative treatments that explicitly compute only the n th-order response. Our MCTDHF results indicate that in order to drive significant (10^{-3} or more) population transfer in

the NO_2 molecule using 1fs pulses, higher-than-2nd-order effects will be encountered at modest intensity ($10^{16} \text{ W cm}^{-2}$).

Furthermore, second order perturbation theory is not a useful tool for determining the conditions for maximum population transfer. Population transfer occurs at a central frequency that is far red-detuned from the optimum at 2nd order. We find that the maximum population transfer occurs 8eV red-detuned from the 2nd order optimum and 6eV red-detuned from any near-edge fine structure, at approximately $3 \times 10^{17} \text{ W cm}^{-2}$. It appears to proceed via nonresonant Raman via the K-edge continuum.

The results will hopefully help guide the selection of experimental conditions under which multidimensional X-ray spectroscopies are most viable. These calculations are the first step toward first-principles calculations of multidimensional x-ray Raman spectroscopies on polyatomic molecules.

V. ACKNOWLEDGMENTS

Calculations have been performed on the Lawrencium supercluster at Lawrence Berkeley National Laboratory (LBNL) under the support of the Laboratory Research Computing program, <http://scs.lbl.gov>. Some work was performed at Lawrence Berkeley National Laboratory, supported by the US Department of Energy Office of Basic Energy Sciences, Division of Chemical Sciences Contract DE-AC02-05CH11231. Further support was provided by the Peder Sather Grant program.

[1] J. D. Biggs, Y. Zhang, D. Healion, and S. Mukamel, *The Journal of Chemical Physics* **136**, 174117 (2012).

[2] S. Mukamel, D. Healion, Y. Zhang, and J. D. Biggs, *Ann. Rev. Phys. Chem.* **64**, 101 (2013).

[3] J. D. Biggs, Y. Zhang, D. Healion, and S. Mukamel, *The Journal of Chemical Physics* **138**, 144303 (2013), <http://dx.doi.org/10.1063/1.479926>.

[4] J. D. Biggs, Y. Zhang, D. Healion, and S. Mukamel, *Proceedings of the National Academy of Sciences* **110**, 15597 (2013).

[5] A. Kirrander, K. Saita, and D. V. Shalashilin, *Journal of Chemical Theory and Computation* **12**, 957 (2016), pMID: 26717255, <http://dx.doi.org/10.1021/acs.jctc.5b01042>.

[6] S. Miyabe and P. Bucksbaum, *Phys. Rev. Lett.* **114**, 143005 (2015).

[7] D. J. Haxton, K. V. Lawler, and C. W. McCurdy, *Phys. Rev. A* **83**, 063416 (2011).

[8] D. J. Haxton and C. W. McCurdy, *Phys. Rev. A* **91**, 012509 (2015).

[9] J. R. Jones, F.-H. Rouet, K. V. Lawler, E. Vecharynski, K. Z. Ibrahim, S. Williams, B. Abeln, C. Yang, W. McCurdy, D. J. Haxton, X. S. Li, and T. N. Rescigno, *Molecular Physics* **114**, 2014 (2016), <http://dx.doi.org/10.1080/00268976.2016.1176262>.

[10] D. J. Haxton, C. W. McCurdy, T. N. Rescigno, K. V. Lawler, J. Jones, B. Abeln, and X. Li, LBNL-AMO-MCTDHF.

[11] M. Kitzler, J. Zanghellini, C. Jungreuthmayer, M. Smits, A. Scrinzi, and T. Brabec, *Phys. Rev. A* **70**, 041401 (2004).

[12] T. Kato and H. Kono, *Chem. Phys. Lett.* **392**, 533 (2004). <http://dx.doi.org/10.1016/j.cplett.2004.03.063>.

[13] T. Kato and H. Kono, *Chem. Phys. Lett.* **392**, 533 (2004). <http://dx.doi.org/10.1016/j.cplett.2004.03.063>.

[14] T. Kato and H. Kono, *Chem. Phys. Lett.* **392**, 533 (2004). <http://dx.doi.org/10.1016/j.cplett.2004.03.063>.

[15] M. Nest, T. Klamroth, and P. Saalfrank, *J. Chem. Phys.* **122**, 124102 (2005).

[16] M. Nest, R. Padmanabhan, and P. Saalfrank, *J. Chem. Phys.* **126**, 214106 (2007).

[17] M. Nest, F. Remacle, and R. D. Levine, *New J. Phys.* **10**, 025019 (2008).

[18] T. Kato and H. Kono, *J. Chem. Phys.* **128**, 184102 (2008).

[19] T. Kato and H. Kono, *J. Chem. Phys.* **128**, 184102 (2008).

[20] T. Kato and H. Kono, *J. Chem. Phys.* **131**, 164118 (2009).

[21] T. Kato, H. Kono, M. Kanno, Y. Fujimura, and K. Yamanouchi, *Laser Physics* **19**, 1712 (2009).

- [22] H. Miyagi and L. B. Madsen, Phys. Rev. A **87**, 062511 (2013).
- [23] T. Sato and K. L. Ishikawa, Phys. Rev. A **88**, 023402 (2013).
- [24] T. Sato and K. L. Ishikawa, Phys. Rev. A **91**, 023417 (2015).
- [25] R. Sawada, T. Sato, and K. L. Ishikawa, Phys. Rev. A **93**, 023434 (2016).
- [26] J. Broeckhove, L. Lathouwers, E. Kesteloot, and P. V. Leuven, Chem. Phys. Lett. **149**, 547 (1988).
- [27] K. Ohta, Phys. Rev. A **70**, 022503 (2004).
- [28] B. Simon, Physics Letters A **71**, 211 (1979).
- [29] D. J. Haxton, K. V. Lawler, and C. W. McCurdy, Phys. Rev. A **86**, 013406 (2012).
- [30] N. Wu and X. Chen, The Journal of Physical Chemistry A **116**, 6894 (2012).
- [31] J. Berkowitz, in *Atomic and Molecular Photoabsorption*, edited by J. Berkowitz (Academic Press, London, 2002) pp. 237 – 316.
- [32] A. Jurgensen and R. G. Cavell, Chemical Physics **257**, 123 (2000).
- [33] T. Gejo, Y. Takata, T. Hatsui, M. Nagasono, H. Oji, N. Kosugi, and E. Shigemasa, Chemical Physics **289**, 15 (2003), decay Processes in Core-excited Species.
- [34] M. Piancastelli, V. Carravetta, I. Hjelte, A. D. Fanis, K. Okada, N. Saito, M. Kitajima, H. Tanaka, and K. Ueda, Chemical Physics Letters **399**, 426 (2004).

